APPROXIMATING NONLINEAR FORCES WITH PHASE-SPACE DECOUPLING

B. Folsom*, E. Laface,
Lund University, Particle Physics Division, Lund, Sweden and
European Spallation Source ERIC, Lund, Sweden

Abstract

Beam tracking software for accelerators typically falls into two categories: fast envelope simulations limited to linear beam optics, and slower multiparticle simulations that can model nonlinear effects. To find a middle ground between these approaches, we introduce virtual coordinates in position and momentum which have a cross-dependency (i.e. $p^* = f(x_0)$ where x_0 is an initial position and p^* is a virtual projection of momentum onto the position axis). This technique approximates multiparticle simulations with a significant reduction in calculation cost.

INTRODUCTION

The software for predicting and correcting beam dynamics in real time is largely dependent on approximations that treat the phase-space density as a single envelope [1, 2], while multiparticle tracking codes that can account for nonlinear forces are more CPU-intensive and only suitable for machine design or offline diagnostics [3, 4]. In developing the ESS Linac Simulator (ELS), our group intends to incorporate nonlinear tracking without sacrificing real-time diagnostics capability.

Expanding on prior works [5, 6], we introduce a multiparticle optimization method by using "virtual" phase-space coordinates that allow for the independent calculation of position and momentum densities. It is important to classify these coordinates as non-physical: they are derived assuming a cross-dependency exists (e.g. $p^* = f(x_0)$, where p^* and x_0 are virtual momentum and real position, respectively).

When used in conjunction with standard techniques for multiparticle tracking, these virtual coordinates allow for the use of monovariate polynomials, which present a significant reduction in the number of required calculations when compared with the bivariate polynomials normally needed.

Although the results to follow consider only multiparticle tests, these techniques may be integrated into beam-envelope simulations by building contour maps from low-particle-count samples.

THEORY

For simplicity, we will begin by considering only transverse motion along a single axis with an initial Gaussian distribution (though we will test the resulting approximation in 2D on various initial distributions).

The starting point for this method, outlined in Ref. [6], involves taking particle count N as an invariant as the position

---

* ben.folsom@esss.se

and momentum envelopes ρ_x and ρ_p evolve:

$$\int \rho_x^L dx_L = \int \rho_x^0 dx_0 = \int \rho_P^L dp_L = \int \rho_P^0 dp_0 = N \ . \quad (1)$$

where ρ_x^L and ρ_x^0 are the respective final and initial position densities, and likewise for the momentum densities.

To exploit this identity, ρ_x^L must be independent of p_0. This can be accomplished using the approximation [7, 8]

$$p_0 \approx -\frac{\alpha}{\beta} x_0 \ , \quad (2)$$

where α and β are the well-known Twiss parameters. Unfortunately, this approximation is only valid if the previous history of the beam is linear (thus maintaining elliptical phase space densities). Since we want an algorithm that remains accurate for iterated nonlinear kicks (which develop irregular density profiles), a new approximation is needed.

Proceeding under the constraint that the initial distribution is Gaussian in both x and p, we can solve Eq. 1 for x_0 and p_0.

$$\int \rho_x^0 dx_0 = \int \rho_P^0 dp_0 \quad (3)$$

$$\frac{1}{2} \operatorname{erf}\left(\frac{\sqrt{2}x_0}{2\,\sigma_{x_0}}\right) = \frac{1}{2} \operatorname{erf}\left(\frac{\sqrt{2}p_0}{2\,\sigma_{p_0}}\right),$$

which yields

$$p_0 = \sqrt{2}\sigma_{p_0} \operatorname{erfinv}\left(\operatorname{erf}\left(\frac{\sqrt{2}x_0}{2\sigma_{x_0}}\right)\right) = x_0 \frac{\sigma_{p_0}}{\sigma_{x_0}} \ . \quad (4)$$

This solution does produce a bigaussian phase-space ellipse, but is unsuitable for approximating p_0 with distributions of an irregular shape.

We continue by guessing that a solution exists for $p_0 = f(x_0)$ for irregularly shaped distributions. Denoting these solutions as p^* and ρ_p^* for momentum and momentum density, respectively, we have

$$\int \rho_P^*(p_0) \, dp^*(x_0) = \int \rho_P^0 dp_0 \ , \quad (5)$$

where it is critical to note that p^* is solely dependent on x_0, while ρ_p^* remains a function of p_0 (and likewise for x^* and ρ_x^*). With the left-hand-side integrand and integration variables decoupled, it follows (for both x^* and p^*):

$$N = x^* \rho_x^* = \int \rho_x^0 dx_0 \quad (6)$$

$$N = p^* \rho_p^* = \int \rho_P^0 dp_0 \ .$$

Exploiting particle-count invariance again, and squaring N, we can assert that

$$N^2 = C = \rho_x^* \rho_p^* x^* p^* \ , \quad (7)$$

and thus

$$\frac{d}{dx_0}C + \frac{d}{dp_0}C = 0 .$$ (8)

We can then simplify, treating all p_0-dependent terms as $f(p_0)$:

$$\begin{aligned} 0 &= \frac{d}{dx_0}C + \frac{d}{dp_0}C & (9)\\ &= \frac{\partial \rho_x^*}{\partial x_0}\left(\rho_p^* x^* p^*\right) + \frac{\partial p^*}{\partial x_0}\left(\rho_x^* \rho_p^* x^*\right) + f(p_0)\\ &= \frac{\partial \rho_x^*}{\partial x_0}\left(\int \rho_p^0 dp_0\, x^*\right)\\ &+ \frac{\partial p^*}{\partial x_0}\left(\int \rho_x^0 dx_0\, \frac{\int \rho_p^0 dp_0}{p^*}\right) + f(p_0) . \end{aligned}$$

Then, dividing by $\int \rho_p^0 dp_0$, the expanded $f(p_0)$ terms become zero and we have:

$$\begin{aligned} 0 &= \frac{\partial \rho_x^{\mathcal{I}}}{\partial x_0} x^* + \frac{\partial p^*}{\partial x_0}\frac{1}{p^*}\int \rho_x^0 dx_0 & (10)\\ &= \frac{\partial \rho_x^*}{\partial x_0} x^* + \frac{\partial p^*}{\partial x_0}\frac{1}{p^*}x^*\rho_x^*\\ &= \left(\frac{\partial \rho_x^*}{\partial x_0} + \frac{\partial p^*}{\partial x_0}\frac{1}{p^*}\rho_x^*\right) . \end{aligned}$$

By reusing Eqn. 6, all p_0 dependence can be eliminated, leaving

$$\frac{\partial p^*}{\partial x_0} = -p^*\frac{\rho_x^0}{\int \rho_x^0 dx_0} = -\frac{p^*\rho_x^0}{\Upsilon_x},\; -\frac{2p^*\rho_x^0}{\Upsilon_x}$$ (11)

where the second solution can be obtained integrating by parts, and, in the case of a Gaussian initial distribution, the placeholder in the denominator is defined as

$$\Upsilon_x \equiv \frac{1}{2}\,\mathrm{erf}\left(\frac{\sqrt{2}x_0}{2\sigma_x}\right) .$$ (12)

Thus, in contrast with Eq. 4, we have an expression where $\frac{\partial p}{\partial x}$ is no longer constant.

We now check the following approximation:

$$p^* \approx -2\sinh\left(\frac{\rho_x^0}{\Upsilon_x}x_0\right)\mathcal{D}$$ (13)

Where we normalize $\mathcal{D}$ using Eq. 4; setting to $p^* \approx -p_0$ near $|x_0| = 0$, leaving

$$p^* \approx 2\sinh\left(\frac{\rho_x^0}{\Upsilon_x}x_0\right)x_0\frac{\sigma_p}{\sigma_x}$$ (14)

which can be shown numerically to agree with Eqn. 11 for $|x_0| \lesssim 6\,\sigma_x$.

At this point, the updated particle position x_L can be calculated using an exponential Lie-operator method [9]:

$$x_L(x_0, p^*) = \{\exp[-t : \mathcal{H}(x_0, p_0):]x_0\}|_{p_0 \to p^*} .$$ (15)

where t is elapsed time in the lab frame and the Hamiltonian for a normal multipole magnet in the transverse plane is

$$\mathcal{H} = \frac{e}{p}\frac{k \cdot \Re(x_0 + iy_0)^n}{a_0^{n-1}\, n!} + \frac{(p_0)^2}{2m} .$$ (16)

Here, e, p, m, and a_0 are the fundamental charge, reference longitudinal momentum, particle mass, and magnet-pole raidus, respectively; $n = 3, 4, 5...$ for sextupoles, octupoles, decapoles, etc; and k has units of $[\mathrm{T}\cdot\mathrm{m}^{-1}]$. In the following sections, longitudinal momentum is normalized to 1 GeV/c and a_0 is set to 20 mm unless otherwise noted.

In implementing Eq. 15, $\mathcal{H}$ must be calculated symbolically first for each element. Then, $p^*(x_0)$ and x_0 are substituted in at each step, reducing the bivariate $x_L(x_0, p_0)$ to a monovariate $x_L(x_0, \sigma_x, \sigma_p)$, where σ_x and σ_p remain constant for a given timestep.

Although an analogous $x^*(p_0)$ can be derived, it is not useful in practice. Specifically, in calculating Eq. 16 in 2D for position and momentum − $x_L(x_0, y_0, p_x^*, p_y^*)$ and $p_{xL}(x^*, y^*, p_{x0}, p_{y0})$ – the resulting x_L expression is dependent on σ_x and σ_{px}, while p_L is dependent on σ_x, σ_y, σ_{px}, and σ_{py}, rendering it computationally inefficient. Other schema involving alternate forms such as $p_L(x_0, p^*)$ have been checked, but the following is found to be most stable, with notable performance gains:

$$\begin{aligned} x_1, y_1, p_{x1}, p_{y1} &\to x_L(x_0, y_0, p_x^*, p_y^*),\, y_L(x_0, y_0, p_x^*, p_y^*)\\ &\quad p_{xL}(x_0, y_0, p_{x0}, p_{x0}),\, p_{yL}(x_0, y_0, p_{x0}, p_{y0})\\ &\qquad\qquad \downarrow\\ x_2, y_2, p_{x2}, p_{y2} &\to x_D(x_1, y_1, p_{x1}, p_{y1}),\, y_D(x_1, y_1, p_{x1}, p_{y1})\\ &\quad p_{xD}(x_1, y_1, p_{x1}, p_{y1}),\, p_{yD}(x_1, y_1, p_{x1}, p_{y1}) \end{aligned}$$ (17)

Where the D subscript denotes a drift space of at least five times the kick length. This effectively limits the technique to a thin-lens approximation. Such drift spaces can be reserved for incorporating space-charge effects, leading to a comparable number of calculation steps using Eq. 17 versus a standard nonlinear beam-physics code.

MULTIPARTICLE SIMULATION

Figure 1 compares the accuracy of multiparticle transformations following Eq. 17 with and without using p^*. Also shown are tests for $p^* = 0$ and a "naive" approximation, where $p^* \approx p_0$ from Eq. 4 is used in the low $|x_0|$ limit of Eq. 14:

$$p^* \approx -x_0\frac{\sigma_p}{\sigma_x} .$$ (18)

To emphasize visible discrepancies, the results shown have their σ values updated after each timestep by taking a new standard deviation. However, if mean absolute deviations are taken instead, an improved matching with the baseline can be observed.

Both the naive and null-momentum approximations fail at $\sigma_p \gtrsim \sigma_x$ (i.e. at energies exceeding 1 GeV). Figure 2 illustrates such a case for 2D Gaussian proton distributions with a kinetic energy of 8 GeV passing through an octupole magnet. In the 2D case, beam parameters were derived relativistically from Twiss parameters and B_0 by normalizing the kinetic term in Eq. 16 to the beam's average kinetic energy then verified against Tracewin [10].
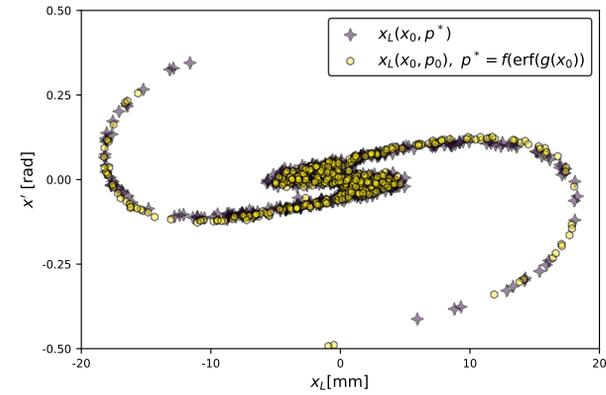
(a) Error-function Approximation
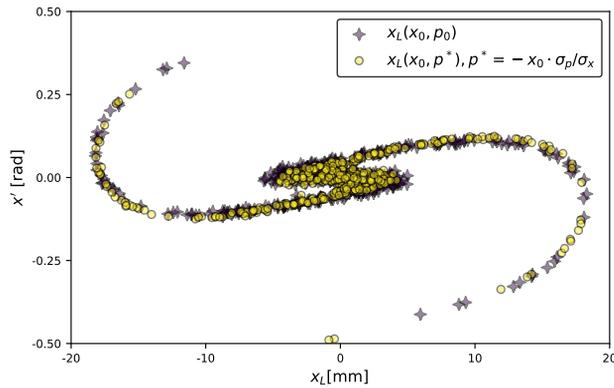
(b) Naive Approximation
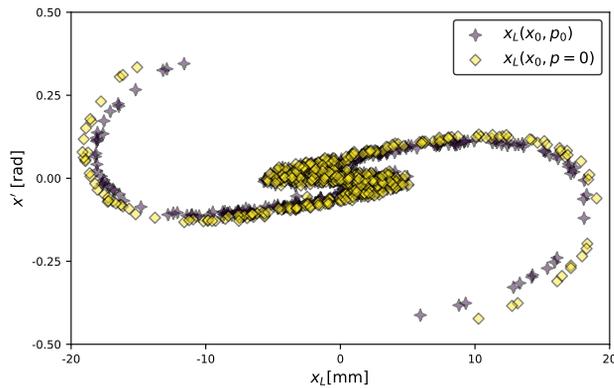
(c) Null-momentum Approximation

Figure 1: Iterated use of Eq. 14 versus standard Lie transport results in 1D for 100,000 protons with initial Gaussian distributions of $\sigma_x = 10$ mm, $\sigma_P = 0.01$ rad (a). Also shown are two alternate p^* approximations: $p^* = x_0 \frac{\sigma_P}{\sigma_x}$ in (b) and $p^* = 0$ in (c). The transport map consists of 200 octupole–drift sections: $B_0 = 10$ [T], $L_{oct} = 0.1$ [mm], $L_{drift} = 1.0$ [mm]. Lie transforms are truncated to fifth order.

CONCLUSION

For the non-null p^* approximations, performance improves with increasing particle count, with increasing mag-
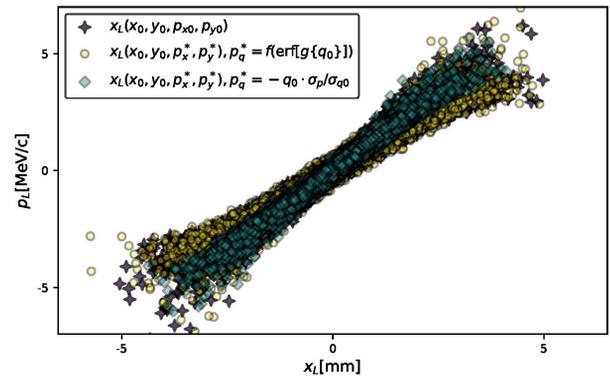
Figure 2: Iterated octupole transforms for 2D Gaussian bunches of 100,000 protons at 8 GeV: $a_0 = 15$ [mm], $\epsilon_\perp = 0.25$ [$\pi \cdot$ mm $\cdot$ mrad], $\beta_\perp = 1$ [mm/($\pi \cdot$ mrad)]. The map consists of 400 kick–drift sections: $B_0 = 12$ T, $L_{oct} = 0.2$ [mm], $L_{drift} = 2$ [mm], for an integrated field strength of 0.211 [T/m^2].
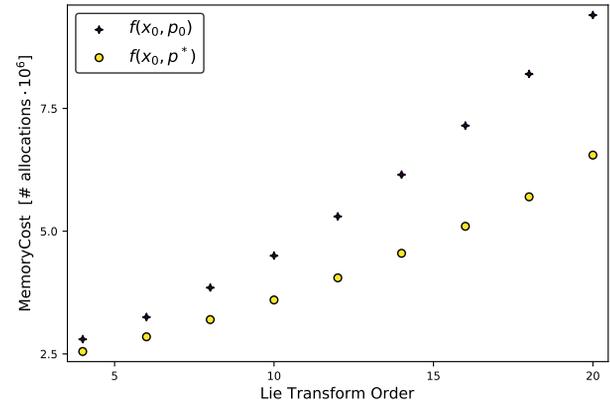
Figure 3: Raw memory-allocation cost for multiparticle simulations with k and L parameters matching those of Fig. 1. Number of particles: 10,000. Number of simulated segments: 5.

netic pole count, and particularly with increased order of Lie-transform series truncation (Fig. 3). Since trajectory variations are negligible beyond a 6th-order truncation in most cases, the average reduction in CPU overhead using Eq. 14 is roughly 15%.

Similar results were obtained for sextupoles, decapoles, and high-order magnets, as well as with waterbag distributions, despite the assumption of a Gaussian shape in deriving Eq. 14. At low energies (or specifically, any low $\frac{\sigma_P}{\sigma_x}$ ratio), all three approximations tested have essentially identical results, with escalating performance in the following order: $p^* = (f[\text{erf}]); \ p^* = -x_0 \cdot \sigma_P/\sigma_x; \ p^* = 0$.

For all the approximations tested, trajectories only became unstable in cases where the momentum of the baseline exceeded $\sim 100\sigma_P$. Thus, the major limitation to this technique is its large drift–kick ratio requirement.

05 Beam Dynamics and Electromagnetic Fields

REFERENCES

[1] H. Grote and F. Schmidt, "Mad-x–an upgrade from mad8," in *Particle Accelerator Conference, 2003. PAC 2003. Proceedings of the*, vol. 5. IEEE, 2003, pp. 3497–3499.

[2] T. Pelaia, C. K. Allen, A. Shishlo, A. Zhukov, Y. Chao, C. Gong, F. Jones, R. Newhouse, P. Chu, D. Maxwell *et al.*, "Open xal status report 2015," in *6th International Particle Accelerator Conference (IPAC2015)*, 2015, pp. 1270–1272.

[3] E. Forest, F. Schmidt, and E. McIntosh, "Introduction to the polymorphic tracking code," *KEK report*, vol. 3, p. 2002, 2002.

[4] R. Ryne, J. Qiang, E. Bethel, I. Pogorelov, J. Shalf, C. Siegerist, M. Venturini, A. Dragt, A. Adelmann, D. Abell *et al.*, "Recent progress on the marylie/impact beam dynamics code," *Lawrence Berkeley National Laboratory*, 2006.

[5] E. Laface, "Non-Linear Dynamics Model for the ESS Linac Simulator," *Proceedings of IPAC 2015, Richmond VA, USA*, May 2015.

[6] B. Folsom and E. Laface, "Fast tracking of nonlinear dynamics in the ess linac simulator via particle-count invariance," in *7th International Particle Accelerator Conference (IPAC'16), Busan, Korea, May 8-13, 2016.* JACOW, Geneva, Switzerland, 2016, pp. 3080–3082.

[7] Y. Yuri, N. Miyawaki, T. Kamiya, W. Yokota, K. Arakawa, and M. Fukuda, "Uniformization of the transverse beam profile by means of nonlinear focusing method," *Physical Review Special Topics-Accelerators and Beams*, vol. 10, no. 10, p. 104001, 2007.

[8] F. Meot and T. Aniel, "Principles of the non-linear tuning of beam expanders," *Nuclear Instruments and Methods in Physics Research Section A: Accelerators, Spectrometers, Detectors and Associated Equipment*, vol. 379, no. 2, pp. 196–205, 1996.

[9] A. J. Dragt, *Lie methods for nonlinear dynamics with applications to accelerator physics.* University of Maryland, Center for Theoretical Physics, Department of Physics, 2015.

[10] D. Uriot and N. Pichoff, "Tracewin documentation," *CEA internap report CEA/DSM/DAPNIA/SEA/2000/45*, 2011.